

OTPrune: Distribution-Aligned Visual Token Pruning via Optimal Transport

Xiwen Chen^{1,2*} Wenhui Zhu^{3*†} Gen Li² Xuanzhao Dong³ Yujian Xiong³ Hao Wang²
 Peijie Qiu⁴ Qingquan Song⁵ Zhipeng Wang⁶ Shao Tang⁷ Yalin Wang³ Abolfazl Razi²
¹ Morgan Stanley, ² Clemson University, ³ Arizona State University,
⁴ Washington University in St. Louis, ⁵ Texas A&M University,
⁶ Rice University ⁷ Florida State University

Abstract

Multi-modal large language models (MLLMs) achieve strong visual–language reasoning but suffer from high inference cost due to redundant visual tokens. Recent work explores visual token pruning to accelerate inference, while existing pruning methods overlook the underlying distributional structure of visual representations. We propose OTPrune, a training-free framework that formulates pruning as distribution alignment via optimal transport (OT). By minimizing the 2-Wasserstein distance between the full and pruned token distributions, OTPrune preserves both local diversity and global representativeness while reducing inference cost. Moreover, we derive a tractable submodular objective that enables efficient optimization, and theoretically prove its monotonicity and submodularity, providing a principled foundation for stable and efficient pruning. We further provide a comprehensive analysis that explains how distributional alignment contributes to stable and semantically faithful pruning. Comprehensive experiments on wider benchmarks demonstrate that OTPrune achieves superior performance–efficiency tradeoffs compared to state-of-the-art methods. The code is available at <https://github.com/xiwenc1/OTPrune>.

1. Introduction

Large multimodal models (LMMs) have emerged as a central paradigm for integrating visual and linguistic understanding [29, 30, 39, 56]. A prominent subset of these models, known as multimodal large language models (MLLMs), extends LLMs by incorporating visual encoders and cross-modal alignment modules. Recent representatives such as LLaVA [29, 30], GPT-4V [34], and Gemini [15] have demonstrated remarkable capabilities in visual question answering, image captioning, and open-ended reasoning [11,

*These authors contributed equally to this paper.

†Now at LinkedIn.

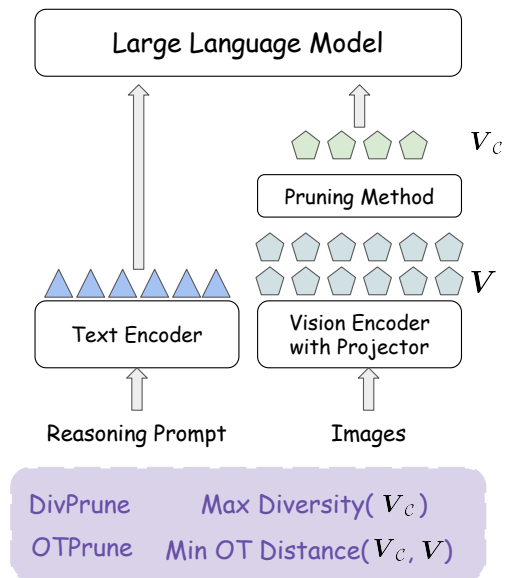


Figure 1. **Overview of the proposed OTPrune framework.** Given visual and textual inputs, a vision encoder with a projector produces image tokens that are fed into a large language model together with text tokens and reasoning prompts. Existing methods, such as *DivPrune*, select tokens by maximizing diversity, which may overlook global representativeness. In contrast, *OTPrune* formulates pruning as *distribution alignment* by minimizing the 2-Wasserstein (optimal transport) distance between the full and pruned token distributions, thereby preserving both local diversity and global structure for efficient and semantically faithful multimodal reasoning.

[25]. These models typically transform both textual and visual inputs into token sequences that are jointly processed by a transformer-based decoder [2, 42]. However, the number of visual tokens in MLLMs often far exceeds that of textual ones. A single image can generate hundreds of patch-level tokens [12], which greatly increases the overall sequence length. Since the self-attention operation in transformers scales quadratically with sequence length [42],

longer multimodal contexts, especially in multi-turn reasoning or dialogue scenarios, lead to substantially higher computational and memory costs during inference [21, 44, 45].

A growing body of work aims to mitigate this bottleneck through visual token pruning, which removes redundant vision tokens while preserving task-relevant semantics. Empirical studies reveal that visual tokens contain redundancy, allowing a large portion of tokens (e.g., 70–90%) to be pruned with little impact on accuracy [10, 28, 40]. A variety of pruning strategies have been proposed to reduce the inference cost of large multimodal models (LMMs), including attention-based [10, 17, 27, 40], calibration-based [28, 50], and trainable approaches [6, 23]. Among them, DivPrune [3] takes a notable step forward by introducing a diversity-driven criterion that favors dissimilar tokens, effectively reducing redundancy and improving generalization. However, diversity alone is not sufficient to ensure representativeness. *While DivPrune enforces separation among selected tokens, it neglects the global relationship between the pruned subset and the full token distribution.* Consequently, the retained subset may fail to capture the underlying covariance structure or semantic coverage of the original vision tokens, especially under high pruning ratios. In other words, diversity promotes dissimilarity within the subset but does not guarantee that the subset faithfully approximates the full feature manifold.

To address this, we argue that effective pruning should account for both local diversity and global distributional alignment. Instead of merely selecting distant tokens, we aim to retain those that best represent the geometry of the full token space. To this end, we propose *OTPrune*, a principled and training-free framework that formulates token pruning as a distribution approximation problem based on *optimal transport (OT) problem*. The selected subset is required to induce a distribution that closely matches that of all tokens, achieved by minimizing the *2-Wasserstein distance* between their empirical distributions. This formulation explicitly aligns the geometric and statistical structures of tokens in the embedding space, ensuring both diversity and representativeness. An overview of the framework is shown in Fig. 1.

However, directly minimizing the Wasserstein distance over discrete subsets is computationally intractable. To solve this, we approximate the token distributions with Gaussian surrogates that match their covariance statistics, leading to a closed-form expression for the 2-Wasserstein distance. We then show that the optimization objective can be effectively optimized by maximizing the log-determinant of the covariance alignment matrix between the selected and full tokens, which serves as a tractable lower-bound surrogate of the trace objective, i.e., *second-order OT surrogate*. The resulting criterion is monotone and submodular, enabling efficient greedy maximization via Cholesky decom-

position with polynomial complexity. In summary, our contributions are as follows:

- We are the first to formulate vision token pruning as a distribution alignment problem by minimizing the 2-Wasserstein distance between the full and pruned token distributions, bridging the gap between local diversity and global representativeness. Empirical analysis confirms that this formulation yields more semantically faithful pruning behavior.
- We derive a tractable *second-order OT surrogate* of the Wasserstein distance that yields a tractable log-determinant objective, which is provably monotone and submodular. Empirical results on synthetic data further demonstrate that this surrogate closely aligns with the true optimal transport objective, providing both theoretical grounding and practical fidelity.
- Comprehensive empirical evaluation and analysis. Across diverse image and video benchmarks, OTPrune achieves superior accuracy–efficiency trade-offs compared to state-of-the-art methods such as FastV, VTW, and DivPrune.

2. Related Works

2.1. Multi-modal large language models (MLLMs)

Multimodal large language models (MLLMs) have recently emerged as a general framework for understanding and reasoning across different modalities, including text, image, audio, and video [11, 15, 25, 29, 30, 35, 56]. They extend large language models (LLMs) with visual or auditory encoders, allowing them to process multimodal inputs in a unified token space. Such models have shown strong performance on tasks like visual question answering, image and video captioning, and visual grounding, as well as more structured tasks such as segmentation and visual editing [46, 47, 54].

2.2. Efficient MLLMs

Recent studies have explored various strategies to improve the inference efficiency of LMMs. Architectural optimization methods include replacing transformer backbones with more efficient state-space models such as Mamba [16, 38], retraining with smaller-scale language models [52, 58], and applying knowledge distillation for model compression [49]. At the inference level, computation skipping [41] and efficient decoding techniques like speculative decoding [14] have been proposed to accelerate reasoning while preserving performance. However, these methods require retraining or architectural changes, which limit their adaptability to general MLLMs. Alternatively, visual token pruning [10, 28, 59] improves efficiency by removing redundant visual tokens from pretrained LMMs without altering the architecture, motivating our scalable and lightweight design.

2.3. Visual Token Pruning

Visual token pruning has become an effective way to reduce the inference cost of large multimodal models (LMMs). Early studies mainly rely on attention-based pruning, where tokens with low attention responses are removed. PruMerge [40] and FastV [10] follow this idea, but later analyses [17, 27] show that attention magnitude does not always reflect true token importance, especially under high pruning ratios. Another direction is calibration-based pruning, where pruning ratios or layers are decided using a small calibration set, as in FitPrune [50] and VTW [28]. FitPrune averages attention maps across samples to build dataset-level statistics, but attention is inherently input-dependent, making these statistics unstable and less generalizable to unseen data. Such methods rely on global heuristics rather than modeling instance-level structure, which limits their robustness across inputs. Fine-tuning-based approaches, such as M³ [6] and TokenPacker [23], improve adaptivity by learning hierarchical or compact token representations, though at significant computational cost. More recently, DivPrune [4] enhances pruning by encouraging token diversity, yet it focuses on local dissimilarity and overlooks global distributional alignment, which is crucial for maintaining representativeness. These observations suggest that effective pruning should balance local diversity and global distributional structure without relying on extra calibration or training. Motivated by this, we introduce an optimal transport-based pruning framework that preserves the global feature distribution while removing redundant tokens. This design enables efficient and semantically faithful pruning, and we further provide theoretical analysis that explains why the optimal transport formulation yields a stable and principled token selection process.

3. Method

3.1. Preliminary

Multimodal inputs typically generate highly redundant token sequences. For a text input, the encoder produces a sequence $\mathbf{T} = \{t_1, \dots, t_n\}$ while for a visual input the encoder produces $\mathbf{V} = \{v_1, \dots, v_m\} \in \mathbb{R}^{m \times d}$. Although n and m may be large, many tokens contribute only marginally to the semantic meaning required for the downstream task. Transmitting all tokens thus wastes valuable communication resources. We can formulate visual token selection as follows. Specifically, we aim to select subsets $\mathcal{C} \subseteq [m]$ such that the selected tokens $\mathbf{V}_{\mathcal{C}} \in \mathbb{R}^{k \times d}$ form semantically representative summaries of their original sequences, where k is the computation budget, i.e., the maximum number of tokens that can be selected, and d denotes the latent dimensions.

Formally, let $f(\cdot)$ denote the downstream LLM task model and $\mathcal{L}(\cdot, \cdot)$ denote a task-specific loss function (e.g.,

cross-entropy for classification or semantic distance for generation). The vision token pruning problem can be written as:

$$\min_{\mathcal{C}} \mathcal{L}(f(\mathbf{T}, \mathbf{V}_{\mathcal{C}}), f(\mathbf{T}, \mathbf{V})) \quad \text{s.t.} \quad |\mathcal{C}| = k. \quad (1)$$

3.2. Pruning as OT Problem

While Eq. 1 formulates pruning in terms of the downstream task loss, such loss is typically infeasible to compute during inference. To enable a task-agnostic formulation, we instead cast pruning as the problem of approximating the distribution of all tokens using that of a pruned subset. We hypothesize that *a closer approximation of the full distribution leads to better downstream task performance*.

Let P denote the distribution induced by the full token set and Q the distribution induced by the selected subset. We assume Q is defined as the empirical distribution of the selected tokens with uniform weights ($\frac{1}{k}$ per token), ensuring that its total mass is normalized to 1. Our goal is to find a subset \mathcal{C} such that Q closely matches P under an appropriate discrepancy measure. Specifically, we focus on minimizing the squared 2-Wasserstein distance:

$$\min_Q \mathcal{W}_2^2(P, Q) = \inf_{\pi \in \Pi(P, Q)} \mathbb{E}_{(x, y) \sim \pi} [\|x - y\|_2^2], \quad (2)$$

which measures the geometric discrepancy between distributions.

Hypothesis Validation. To validate our hypothesis that a better distributional approximation leads to improved downstream performance, we conduct a preliminary study using LLaVA 1.5-7B across 11 multimodal reasoning and understanding benchmarks (see Sec. 5.1 for details of datasets). Given a sequence of m tokens, we sample k tokens ($k < m$) using several simple index-based strategies. *First-K sampling* selects the first k tokens from the sequence, retaining the earliest portion. *Last-K sampling* keeps the last k tokens, focusing on the most recent part of the sequence. *Uniform index sampling* evenly samples from the index range, ensuring that the selected k tokens are uniformly distributed across the entire sequence. We also include *DivPrune* [4], the recent state-of-the-art pruning method, and random selection for comparison. For each strategy, we compute two rankings: (i) the rank of the OT distance between the selected subset and the full token set (lower rank indicates closer distributional alignment), and (ii) the rank of the downstream task performance (higher accuracy corresponds to a lower rank). We then calculate Spearman’s rank correlation between these two rankings. As shown in Fig. 2, the strong positive correlation confirms that subsets achieving smaller OT distances tend to yield higher downstream performance, supporting our distribution-alignment hypothesis.

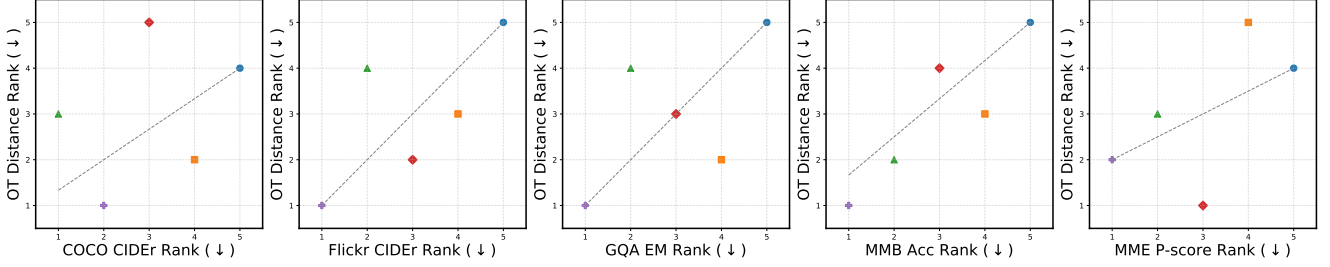


Figure 2. **Correlation between OT distance and downstream performance.** We evaluate several manually designed selection strategies (*First-K*, *Last-K*, *Uniform*, and *Random*) along with the SOTA method *DivPrune* [4]. For each strategy, we compute the OT distance between the selected subset and the full token set and measure downstream performance across 11 multimodal benchmarks. Both OT distance (lower distance \Rightarrow lower rank) and task performance (higher score \Rightarrow lower rank) are ranked to compute Spearman’s correlation. A strong positive correlation confirms that smaller OT distance corresponds to higher performance.

3.3. OTPrune Selector

For analytic tractability, we approximate the OT distance by a Gaussian surrogate. Motivated by moment-matching approaches [7], we adopt a second-order approximation. Following the analytical convenience in [51], we use zero-mean Gaussians to represent the true token distributions: $P \approx \mathcal{N}(0, \Sigma)$ and $Q \approx \mathcal{N}(0, \Sigma_C)$. In this case, the squared 2-Wasserstein distance in Eq. 2 admits a closed form:

$$\mathcal{W}_2^2(P, Q) = \text{tr}(\Sigma) + \text{tr}(\Sigma_C) - 2 \text{tr}\left((\Sigma^{1/2}\Sigma_C\Sigma^{1/2})^{1/2}\right). \quad (3)$$

To avoid scaling bias and ensure fair comparison across features, we normalize each embedding dimension to unit variance. This yields $\Sigma_{ii} = 1$ and $\text{tr}(\Sigma) = d$, leaving the distance primarily sensitive to mismatches in covariance structure rather than absolute scaling. Equivalently, we are maximizing the following objective function $f(\mathcal{C})$:

$$\max_{\mathcal{C}} \underbrace{\left(\text{tr}(\Sigma^{1/2}\Sigma_C\Sigma^{1/2})^{1/2}\right)^2}_{f(\mathcal{C})} \quad \text{s.t.} \quad |\mathcal{C}| = k. \quad (4)$$

Although \mathcal{W}_2^2 is a principled distortion metric, it is still computationally expensive to optimize over discrete subsets.

To this end, instead of directly optimizing the original objective, we consider a more *tractable lower bound*. Specifically, we introduce the γ -log-determinant operator for a positive semidefinite square matrix \mathbf{X} :

$$\Psi(\mathbf{X}) = \log \det(\mathbf{I} + \gamma\mathbf{X}) = \sum_{i=1}^d \log(1 + \gamma\lambda_i), \quad (5)$$

where $\{\lambda_i\}$ are the eigenvalues of \mathbf{X} and $\gamma > 0$ is a fixed scaling parameter. Since \mathbf{X} is positive semidefinite (so $\lambda_i \geq 0$), we have the following inequalities (See Appendix A.1 for the proof),

$$\Psi(\mathbf{X}) \leq \gamma \text{tr}(\mathbf{X}) \leq \gamma(\text{tr}(\mathbf{X}^{1/2}))^2, \quad (6)$$

indicating that $\Psi(\mathbf{X})$ serves as a lower bound of the trace objective. For small γ , this bound becomes tight because $\log(1 + \gamma\lambda_i) \approx \gamma\lambda_i$ when x is close to zero, leading to $\Psi(\mathbf{X}) \approx \gamma \text{tr}(\mathbf{X})$. Thus, since $\Sigma^{1/2}\Sigma_C\Sigma^{1/2} \succeq 0$, we can safely apply $\mathbf{X} = \Sigma^{1/2}\Sigma_C\Sigma^{1/2}$ to the above inequality and obtain the following surrogate objective¹:

$$\max_{\mathcal{C}} \underbrace{\log \det(\mathbf{I} + \gamma \Sigma^{1/2}\Sigma_C\Sigma^{1/2})}_{\tilde{f}(\mathcal{C})}. \quad (7)$$

Since $\Sigma \approx \frac{\mathbf{V}^T\mathbf{V}}{m}$, $\Sigma_C \approx \frac{\mathbf{V}_C^T\mathbf{V}_C}{k}$, and by leveraging the *Sylvester’s determinant identity* $\log \det(\mathbf{I} + \mathbf{X}\mathbf{X}^T) = \log \det(\mathbf{I} + \mathbf{X}^T\mathbf{X})$ for any matrix \mathbf{X} [36], we can rewrite Eq. 7 as

$$\begin{aligned} & \log \det(\mathbf{I} + \gamma \Sigma^{1/2}\Sigma_C\Sigma^{1/2}) \quad (8) \\ & \approx \log \det\left(\mathbf{I} + \frac{\gamma}{mk} (\mathbf{V}^T\mathbf{V})^{1/2}\mathbf{V}_C^T\mathbf{V}_C(\mathbf{V}^T\mathbf{V})^{1/2}\right) \\ & = \log \det\left(\mathbf{I} + \frac{\gamma}{mk} \mathbf{V}_C(\mathbf{V}^T\mathbf{V})^{1/2}(\mathbf{V}^T\mathbf{V})^{1/2}\mathbf{V}_C^T\right) \\ & = \log \det\left(\mathbf{I} + \frac{\gamma}{mk} \mathbf{V}_C\mathbf{V}^T\mathbf{V}\mathbf{V}_C^T\right) \\ & = \log \det\left(\mathbf{I} + \frac{\gamma}{mk} \tilde{\mathbf{V}}_C\tilde{\mathbf{V}}_C^T\right), \end{aligned}$$

where $\tilde{\mathbf{V}}_C = \mathbf{V}_C\mathbf{V}^T$ and $\tilde{\gamma} = \frac{\gamma}{mk}$. Therefore, now we are targeting to maximize $\log \det(\mathbf{I} + \tilde{\gamma}\mathbf{V}_C\mathbf{V}^T\mathbf{V}\mathbf{V}_C^T)$, subject to $|\mathcal{C}| = k$. Notably, this objective defines a monotone submodular set function with respect to \mathcal{C} (See Appendix A.2 for the proof). Due to optimizing this objective being NP-hard, we therefore adopt a greedy approximation strategy based on Cholesky decomposition [8]. Under this strategy, the t -th greedy iteration updates the $(m - t)$ remaining items, each requiring an $O(t)$ inner product between

¹We deliberately avoid using $\mathbf{X} = (\Sigma^{1/2}\Sigma_C\Sigma^{1/2})^{1/2}$ to compute $\Psi(\mathbf{X})$ because evaluating matrix square roots (e.g., via SVD or eigendecomposition) would incur significant overhead during greedy subset selection. Instead, we adopt $\mathbf{X} = \Sigma^{1/2}\Sigma_C\Sigma^{1/2}$, which yields a tractable surrogate with the same monotonicity and submodularity properties, while preserving the lower-bound relationship in Eq. 6.

the current Cholesky coefficients, resulting in a per-iteration cost of $O((m-t)t)$. Summing over $t = 1, \dots, k$ gives a total greedy complexity of $O(mk^2)$. Formally, we give the algorithmic summary in Algorithm 1. **Code is provided in the supplementary material.**

Theoretical Bound. Due to the submodular nature of the objective function defined in Eq. 6, the greedy selection procedure enjoys the classical $(1 - 1/e)$ approximation worst-case guarantee with respect to the optimal subset [19]:

$$\tilde{f}(\mathcal{C}_{\text{greedy}}) \geq (1 - e^{-1}) \tilde{f}(\mathcal{C}^*), \quad (9)$$

where $\tilde{f}(\mathcal{C})$ denotes the objective value for a subset \mathcal{C} computed from Eq. 6, $\mathcal{C}_{\text{greedy}}$ is the subset selected by our algorithm, and \mathcal{C}^* is the optimal subset. Since Eq. 6 serves as a close surrogate to the original objective in Eq. 4, the same approximation bound is expected to hold in practice. Moreover, as demonstrated in Section 4, our empirical analysis shows that the greedy algorithm often achieves a substantially higher optimality ratio than the theoretical $(1 - 1/e)$ bound.

Algorithm 1 OTPrune (See Appendix B for details)

Require: Vision tokens $\mathbf{V} \in \mathbb{R}^{m \times d}$, size k , scalar $\tilde{\gamma}$

Ensure: Selected index set \mathcal{C}

- 1: Precompute $\tilde{\mathbf{V}} = \mathbf{V}\mathbf{V}^\top$, with rows \mathbf{w}_i^\top for $i = 1, \dots, m$, i.e. $\mathbf{w}_i = \tilde{\mathbf{V}}[i, :]^\top$
 - 2: Initialize $\mathcal{C} \leftarrow \emptyset$, $d_i^2 \leftarrow 1 + \tilde{\gamma} \|\mathbf{w}_i\|_2^2$ for all i , and $\mathbf{c}_i \leftarrow \emptyset$
 - 3: **while** $|\mathcal{C}| < k$ **do**
 - 4: $j \leftarrow \arg \max_{i \notin \mathcal{C}} d_i^2$
 - 5: $\mathcal{C} \leftarrow \mathcal{C} \cup \{j\}$
 - 6: **for each** $i \notin \mathcal{C}$ **do**
 - 7: $e_i \leftarrow \frac{\tilde{\gamma} \langle \mathbf{w}_j, \mathbf{w}_i \rangle - \langle \mathbf{c}_j, \mathbf{c}_i \rangle}{d_j}$
 - 8: $\mathbf{c}_i \leftarrow [\mathbf{c}_i \ e_i]$
 - 9: $d_i^2 \leftarrow d_i^2 - e_i^2$
 - 10: **end for**
 - 11: **end while**
 - 12: **return** \mathcal{C}
-

4. Empirical Analysis of the Algorithm

To assess the empirical behavior of the proposed *OTPrune* algorithm, we conduct controlled experiments using synthetic data. Specifically, we generate multiple datasets with varying numbers of samples and feature dimensions. For each dataset, we also vary the number of selected samples to simulate different pruning ratios. When both the total number of samples n and the selected subset size k are relatively small, exhaustive subset evaluation is tractable, allowing us to enumerate all possible combinations $\binom{m}{k}$. In

larger settings, where exhaustive search becomes infeasible, we adopt a Monte Carlo strategy by randomly sampling 10 million candidate subsets to approximate the full search space.

In this analysis, rather than evaluating the approximate objective $\tilde{f}(\cdot)$, we directly evaluate distribution distance via the original objective function defined in Eq. 4, i.e., $f(\cdot)$ and assess the performance of each method (*OTPrune* and *DivPrune*) using two metrics: (i) the *win rate*, and (ii) the *optimality ratio*, defined as $f(\tilde{\mathcal{C}})/f(\mathcal{C}^*)$, where $\tilde{\mathcal{C}}$ denotes the subset selected by the corresponding algorithm and \mathcal{C}^* represents the optimal subset. The *win rate* measures the proportion of all possible subset selection strategies whose objective value $f(\mathcal{C})$ is lower than that achieved by the given method:

$$\text{WinRate} = \frac{|\{\mathcal{C} \subseteq [m], |\mathcal{C}| = k \mid f(\tilde{\mathcal{C}}) > f(\mathcal{C})\}|}{\binom{m}{k}}.$$

This metric reflects how frequently a method’s selected subset surpasses alternative strategies across the entire combinatorial space. It can also be interpreted probabilistically as the expected dominance probability under random subset selection, since the uniform random subset samples each \mathcal{C} with equal probability: $\text{WinRate} = \Pr_{\mathcal{C} \sim \text{Uniform}(\binom{[m]}{k})} [f(\tilde{\mathcal{C}}) > f(\mathcal{C})]$. Hence, the win rate provides an intuitive statistical interpretation of how consistently an algorithm dominates random selection, while the optimality ratio quantifies its proximity to the best possible subset.

Table 2 summarizes the results across different synthetic configurations. For each setting, we compare *OTPrune* and *DivPrune*, and include the implicit random selection baseline, whose expected performance equals the mean of $f(\mathcal{C})$ across all subsets. Both methods substantially outperform random selection, achieving high win rates and optimality ratios that confirm the effectiveness of structured token selection over naive sampling. However, *OTPrune* consistently achieves markedly higher scores than *DivPrune*, particularly in low-dimensional or small-sample regimes where diversity-only criteria are less reliable. Even when the search space becomes large, *OTPrune* maintains near-perfect performance (e.g., achieving 100% win rate and 100% optimality ratio in high-dimensional cases), demonstrating that our submodular approximation closely aligns with the original OT objective. Importantly, both methods empirically achieve optimality ratios exceeding the theoretical $(1 - 1/e)$ bound guaranteed for the maximization problem, indicating that the bound is conservative in practice. Nevertheless, *OTPrune* consistently attains ratios much closer to 1.0 across all settings, showing that its distribution-aware formulation more effectively captures global structure and achieves near-optimal performance. These results empirically confirm that modeling distribu-

Table 1. Comparison of *OTPrune* (ours) with *one-shot*, *adaptive*, and *finetuning* methods on 11 benchmarks. DivPrune* matches the PruMerge selection ratio. Following DivPrune, one-shot methods use a fixed token budget (9.8% retained), with TFLOPs acting as a complementary hardware-agnostic reference. The *Avg. Rank* ↓ is computed across all methods, and the *One-shot Rank* ↓ only among one-shot methods. *OTPrune* consistently achieves the best ranks. •: Finetuning used, △: Calibration used.

	Method	TFLOP (ratio %)	COCO CIDEr	Flickr CIDEr	GQA EM	MMB Acc	MME P-score	MMMU Acc	Nocaps CIDEr	OKVQA EM	POPE F1	SQA EM	SEEDB Acc	Avg. Rank ↓	One-shot Rank ↓	
LLaVA 1.5-7B	Original	3.228 (100.00)	1.10	0.75	61.96	64.09	1506	36.44	1.06	53.39	85.84	69.41	66.17	–	–	
	<i>Category: One-shot Pruning Methods</i>															
	VTW [28]	0.603 (18.46)	0.05	0.03	38.94	21.31	681	32.60	0.03	18.64	25.35	65.29	36.13	8.23	3.41	
	FastV [10]	0.514 (15.69)	0.06	0.03	38.73	20.62	696	32.00	0.04	18.32	32.84	65.15	35.69	8.41	3.59	
	DivPrune	0.512 (15.63)	0.96	0.62	56.85	59.19	1328	35.89	0.92	46.98	86.02	68.27	59.47	3.23	1.64	
	OTPrune (Ours)	0.512 (15.63)	1.00	0.68	56.62	60.40	1368	35.44	0.99	47.09	79.59	68.42	59.31	2.36	1.36	
	<i>Category: Adaptive Pruning Methods</i>															
	PruMerge [40]	Variable	0.77	0.50	51.30	54.47	1259	35.11	0.73	41.74	66.89	68.91	53.26	6.09	–	
	DivPrune*	Variable	0.91	0.56	55.25	58.16	1330	35.44	0.87	44.38	83.06	67.87	57.88	4.73	–	
	<i>Category: Finetuning-based Methods</i>															
	FitPrune [△] [50]	0.513 (15.65)	0.90	0.56	52.39	57.65	1197	36.00	0.86	42.53	60.89	68.02	54.84	5.59	–	
	M ³ * [6]	0.512 (15.63)	1.00	0.67	60.81	65.81	1391	31.80	0.95	55.12	86.33	64.65	64.93	2.68	–	
	PruMerge-LoRA*	Variable	0.96	0.63	55.96	59.88	1334	34.89	0.90	47.99	77.13	68.32	57.93	3.68	–	
	LLaVA 1.5-13B	Original	6.281 (100.00)	1.16	0.80	63.33	68.64	1522	35.67	1.09	58.28	85.99	72.88	66.82	–	–
<i>Category: One-shot Pruning Methods</i>																
VTW [28]		1.030 (16.16)	0.08	0.05	39.71	21.91	622	32.10	0.05	22.49	0.40	66.24	38.59	6.00	4.00	
FastV [10]		1.003 (15.73)	0.38	0.18	44.98	37.80	942	35.11	0.33	32.14	30.02	69.96	44.95	4.82	2.91	
DivPrune		1.002 (15.71)	1.00	0.66	57.29	63.40	1407	34.89	0.95	53.29	83.43	72.34	62.04	2.14	1.91	
OTPrune (Ours)		1.002 (15.71)	1.03	0.71	57.11	65.55	1411	37.00	1.01	54.56	79.39	73.82	62.08	1.27	1.18	
<i>Category: Adaptive Pruning Methods</i>																
PruMerge [△] [40]	Variable	0.80	0.53	52.01	58.93	1256	36.56	0.77	49.15	64.36	72.53	56.10	3.64	–		
DivPrune*	Variable	0.94	0.59	56.09	61.77	1344	34.89	0.91	50.86	79.60	71.34	60.00	3.14	–		
LLaVA 1.6-7B	Original	11.849 (100.00)	1.00	0.68	64.28	67.01	1520	36.44	0.88	44.20	86.38	70.15	70.16	–	–	
	<i>Category: One-shot Pruning Methods</i>															
	VTW [28]	1.318 (11.23)	0.06	0.03	38.62	19.76	606	31.30	0.03	8.66	7.13	65.74	37.48	3.82	3.82	
	FastV [10]	1.327 (11.30)	0.06	0.03	38.79	20.36	619	32.56	0.04	8.80	7.78	65.49	37.62	3.18	3.18	
	DivPrune	1.266 (10.79)	0.89	0.61	58.69	63.49	1362	37.11	0.76	41.92	82.97	68.57	64.11	1.77	1.77	
OTPrune (Ours)	1.266 (10.79)	0.89	0.64	60.28	63.75	1414	38.33	0.84	43.26	81.41	68.07	64.79	1.23	1.23		

Table 2. Comparison between OTPrune and DivPrune on synthetic datasets with varying numbers of samples (m), feature dimensions (d), and selected subset sizes (k). The first two configurations are evaluated exhaustively over all $\binom{m}{k}$ combinations, while the last three configurations use Monte Carlo estimation with 10 million different subsets to approximate the full combinatorial space.

Configuration			Performance		
m	d	k	Method	Win Rate	Optimality Ratio
20	10	5	DivPrune	60.14	74.53
			OTPrune	94.56	87.81
30	20	10	DivPrune	84.62	76.48
			OTPrune	99.49	93.98
100	50	30	DivPrune	88.77	92.20
			OTPrune	99.99	100.00
100	80	50	DivPrune	92.14	95.80
			OTPrune	100.00	100.00
1000	256	100	DivPrune	97.59	97.71
			OTPrune	100.00	100.00

tional alignment yields stronger representational coverage and robustness than diversity-only strategies.

5. Experiment

In this section, we will delve into a comprehensive comparison of our proposed method with prior works on downstream tasks. Additionally, we give an analysis of the efficiency of OTPrune and include an ablation study to examine its key components.

5.1. Experimental Settings

Datasets. We selected a comprehensive set of common tasks and 11 datasets aimed at multimodal reasoning and understanding involving ScienceQA-IMG (SQA) [32], POPE [24], MME [57], MMB [31], GQA [18], MMMU [53], Flickr30k [37], SeedBench (SEEDB) [22], Nocaps [1], OKVQA [33], and COCO-2017 [26]. These datasets encompass a wide range of tasks, including captioning, multiple-choice Question Answering (QA), and open-ended QA based on text and image inputs.

Evaluation metrics. Consistent with prior works [4], CIDEr score [43] is used for evaluating captioning tasks, and Exact Match (EM), Accuracy (Acc), F1, Perception Score (P-score) [57] and GPT-assisted [13] score are used for QA tasks. Furthermore, Wu-Palmer similarity (WUPS) score [48] and GPT-assisted score [13] is used for open-ended QA. For all task performance metrics used in this paper, higher values indicate better performance. Following

the earlier works in [10, 28, 50], we also report the computational requirement, measured in TFLOPs (consistency with [4]). Lower values indicate better results.

Baselines and Models. Following [4], we consider five baselines: FastV [10], PruMerge [40], VTW [28], FitPrune [50], M³ [6], and DivPrune [4]. Among these, we consider FastV, VTW, DivPrune, and PruMerge as our **main competitors** as they are plug-and-play for each sample and do not rely on any further costly finetuning or calibration process. FastV, VTW, and DivPrune are *one-shot*, meaning they require a predefined pruning ratio shared across all samples, whereas PruMerge is *adaptive*, dynamically determining how many and which tokens to retain based on each image’s content rather than relying on a fixed threshold or ratio. However, for the sake of completeness, we also report performance comparison with respect to one finetuning-based (M³) and one calibration-based (FitPrune) method. Note that, VTW, by default, requires calibration to determine the best layer for a given task. However, doing that does not allow us to set a specific TFLOP ratio, complicating the comparison. Hence, whenever required, we disable the calibration of VTW to select the layer that matches the FLOP requirement of a particular experiment.

Implementation. We test OTPrune and the baselines with different popular LMMs, involving LLaVA 1.5-7B [30]², LLaVA 1.5-13B [30]³, and LLaVA 1.6-7B⁴ (also known as LLaVA-NeXT [29]), to demonstrate the generality of DivPrune. For each tested model and task, we report only the relevant subset of baseline that is applicable to that specific model and task, alongside our results. All the tested LMMs used CLIP vision encoder [39]. LLaVA 1.5 model uses 576 visual tokens to represent images. LLaVA 1.6 converts each image into a varying number of patches, resulting in 3-5 times more visual tokens compared to LLaVA 1.5. We used 1 × A100 GPU with 80GB VRAM for all the experiments in this paper. Additionally, we used the lmms-evals package [55] for running these benchmarks for all the baselines and models. All results are obtained with a batch size of 1. For the metrics that require ChatGPT API access, the model is set to “gpt-4o-mini”.

5.2. Main Results

Table 1 summarizes the quantitative comparison of OTPrune against existing pruning approaches across 11 multimodal benchmarks. Among training-free one-shot baselines (VTW [27], FastV [9], and DivPrune [4]), OTPrune consistently achieves the top rank. For LLaVA 1.5-7B, OTPrune improves the average rank from 3.23 (DivPrune) to 2.36 and the one-shot rank from 1.64 to 1.36, yielding higher CIDEr and QA scores at roughly 15% of the original

FLOPs. On LLaVA 1.5-13B, the average rank drops from 2.14 to 1.27 and the one-shot rank to 1.18. For LLaVA 1.6-7B, OTPrune maintains the best performance (Avg. Rank = 1.23) at approximately 11% computation. These improvements confirm that distribution-aware selection via optimal transport yields better semantic coverage than diversity-only pruning. Adaptive strategies such as PruMerge [40] and DivPrune* remain directly comparable, as they require no additional training. OTPrune achieves comparable or higher accuracy while maintaining consistent efficiency, indicating that distributional alignment can provide the same adaptivity benefits without explicit layer- or ratio-specific calibration. Approaches such as FitPrune [50] and M³ [6] involve additional training or external calibration datasets, making them not strictly comparable to our one-shot setting. Nevertheless, OTPrune attains similar or superior task performance without any retraining, underscoring its practicality as a fully training-free alternative.

Statistic Test. To assess the consistency and significance of performance differences across multiple datasets and evaluation metrics, we conducted a non-parametric statistical analysis based on the Wilcoxon signed-rank test. Specifically, we computed the *relative* percentage improvement of every metric with respect to its baseline configuration, i.e., DivPrune. The Wilcoxon signed-rank test was then applied across all metrics to evaluate whether the median improvement was significantly greater than zero (one-sided test). As shown in the right table, our method achieves a *p*-value of 0.028, indicating that it statistically outperforms DivPrune, the previous state-of-the-art.

Comparison	<i>p</i> -value
OTPrune vs DivPrune	0.028

In summary, OTPrune delivers the strongest accuracy–efficiency trade-off among all directly comparable pruning methods and remains competitive even against fine-tuned variants.

5.3. Analysis

Comparison with Diversity-based Methods. For a comprehensive evaluation, we conduct experiments using LLaVA 1.5-13B across 11 multimodal benchmarks with varying token ratios {0.05, 0.098, 0.15, 0.2}. In addition to OTPrune and the state-of-the-art DivPrune [4], we include the widely used diversity-based selection method, Determinantal Point Process (DPP) [20], as well as *Random sampling*. We report both the absolute task performance for each dataset and the *relative performance*, defined as the ratio between pruned and original model performance (*pruned/original*), to account for scale differences across metrics. To further validate our hypothesis, we compute the OT distance between each selected subset and the full token set. For readability, we present the *relative distance* normal-

²<https://huggingface.co/liuhaotian/llava-v1.5-7B>

³<https://huggingface.co/liuhaotian/llava-v1.5-13b>

⁴<https://huggingface.co/liuhaotian/llava-v1.6-vicuna-7b>

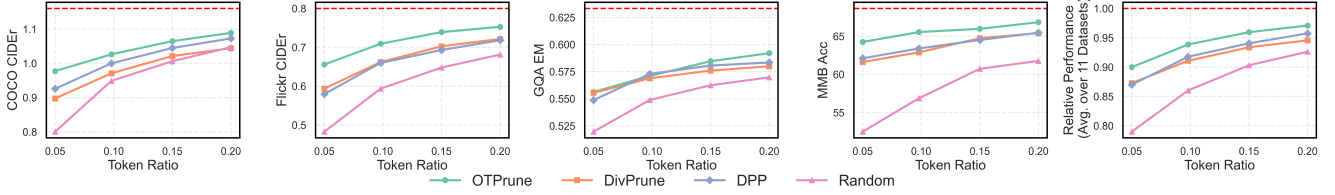


Figure 3. **Comparison with diversity-based methods using LLaVA 1.5-13B.** We evaluate *OTPrune*, *DivPrune* [4], *DPP* [20], and *Random sampling* across 11 multimodal benchmarks under different pruning ratios $\{0.05, 0.098, 0.15, 0.2\}$. We report both absolute performance and *relative performance*, defined as the ratio between pruned and original model performance ($pruned/original$). We also compute the OT distance between each subset and the full token set and visualize the *relative distance* normalized by *OTPrune*, i.e., $f(\mathcal{C}_{method})/f(\mathcal{C}_{OTPrune})$.

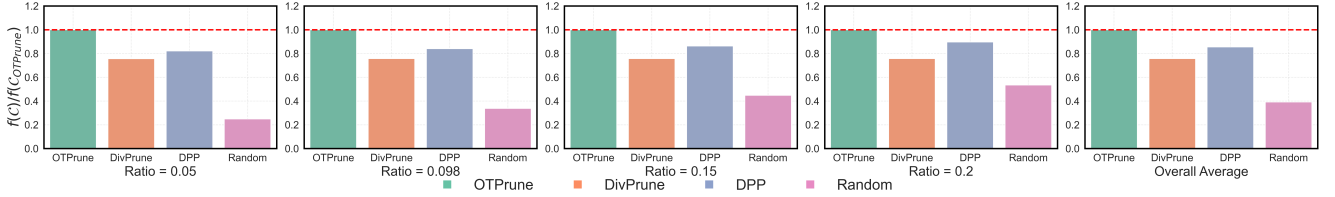


Figure 4. **Relative OT distance comparison across pruning methods.** We evaluate *OTPrune*, *DivPrune* [4], *DPP* [20], and *Random sampling* using LLaVA 1.5-13B across 11 multimodal benchmarks under different token ratios $\{0.05, 0.098, 0.15, 0.2\}$. Each bar shows the relative OT distance normalized by *OTPrune*, i.e., $f(\mathcal{C}_{method})/f(\mathcal{C}_{OTPrune})$, where lower values indicate closer alignment with the original token distribution. **OTPrune consistently achieves the smallest OT distance across all ratios, demonstrating superior distributional fidelity. The last panel reports the overall average across all 11 datasets.**

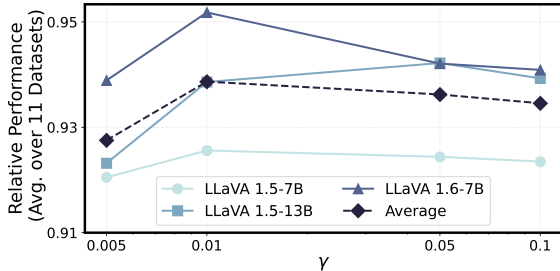


Figure 5. Sensitivity analysis of the balancing coefficient γ .

ized by *OTPrune*, i.e., $f(\mathcal{C}_{method})/f(\mathcal{C}_{OTPrune})$. As shown in Fig. 3 and Fig. 4, *OTPrune* consistently achieves the lowest OT distance and highest relative performance across all token ratios, with clear advantages that persist even in the averaged results over 11 datasets.

Sensitivity of γ . We further investigate the sensitivity of the balancing coefficient γ in Eq. (7) that controls the trade-off between the OT loss and the token selection regularization. We experiment with $\gamma \in \{0.005, 0.01, 0.05, 0.1\}$ using LLaVA 1.5-7B, LLaVA 1.5-13B, and LLaVA 1.6-7B across 11 multimodal benchmarks. As shown in Fig. 5, the overall trend remains stable across models, demonstrating that *OTPrune* is robust to the choice of γ . Performance slightly improves when γ increases from 0.005 to 0.01, indicating a beneficial balance between distributional alignment

and sparsity, and then plateaus for larger values. This suggests that *OTPrune* does not require extensive hyperparameter tuning, and $\gamma = 0.01$ serves as a good default across model scales.

6. Conclusion

In this work, we proposed *OTPrune*, a principled token pruning framework formulated as an optimal transport problem. Unlike prior task-specific or heuristic pruning approaches, *OTPrune* aligns the distribution of pruned tokens with that of the full token set, offering a task-agnostic and geometry-aware objective. We show that minimizing the Wasserstein distance effectively preserves the representational structure of visual-language models. Extensive experiments on 11 multimodal reasoning and understanding benchmarks validate that better distributional approximation yields stronger performance. *OTPrune* consistently outperforms diversity-based and random baselines across pruning ratios and model scales. Our analysis further shows that OT distance correlates strongly with downstream accuracy, providing an interpretable metric for pruning quality. The method is robust to the trade-off parameter γ , requiring minimal tuning. Moreover, *OTPrune* generalizes well across LLaVA variants, confirming its scalability and broad applicability. We hope this work inspires further research on distribution-aware pruning that improves efficiency without compromising performance in MLLMs.

References

- [1] Harsh Agrawal, Karan Desai, Yufei Wang, Xinlei Chen, Rishabh Jain, Mark Johnson, Dhruv Batra, Devi Parikh, Stefan Lee, and Peter Anderson. Nocaps: Novel object captioning at scale. In *Proceedings of the IEEE/CVF international conference on computer vision*, pages 8948–8957, 2019. 6
- [2] Jean-Baptiste Alayrac, Jeff Donahue, Pauline Luc, Antoine Miech, Iain Barr, Yana Hasson, Karel Lenc, Arthur Mensch, Katherine Millican, Malcolm Reynolds, et al. Flamingo: a visual language model for few-shot learning. *Advances in neural information processing systems*, 35:23716–23736, 2022. 1
- [3] Saeed Ranjbar Alvar, Gursimran Singh, Mohammad Akbari, and Yong Zhang. Divprune: Diversity-based visual token pruning for large multimodal models. In *Proceedings of the Computer Vision and Pattern Recognition Conference*, pages 9392–9401, 2025. 2
- [4] Saeed Ranjbar Alvar, Gursimran Singh, Mohammad Akbari, and Yong Zhang. Divprune: Diversity-based visual token pruning for large multimodal models. In *Proceedings of the Computer Vision and Pattern Recognition Conference*, pages 9392–9401, 2025. 3, 4, 6, 7, 8
- [5] Francis Bach et al. Learning with submodular functions: A convex optimization perspective. *Foundations and Trends® in machine learning*, 6(2-3):145–373, 2013. 11
- [6] Mu Cai, Jianwei Yang, Jianfeng Gao, and Yong Jae Lee. Matryoshka multimodal models. In *Workshop on Video-Language Models@ NeurIPS 2024*, 2024. 2, 3, 6, 7
- [7] Chao Chen, Zhihang Fu, Zhihong Chen, Sheng Jin, Zhaowei Cheng, Xinyu Jin, and Xian-Sheng Hua. Homm: Higher-order moment matching for unsupervised domain adaptation. In *Proceedings of the AAAI conference on artificial intelligence*, pages 3422–3429, 2020. 4
- [8] Laming Chen, Guoxin Zhang, and Eric Zhou. Fast greedy map inference for determinantal point process to improve recommendation diversity. *Advances in Neural Information Processing Systems*, 31, 2018. 4
- [9] Liang Chen, Haozhe Zhao, Tianyu Liu, Shuai Bai, Junyang Lin, Chang Zhou, and Baobao Chang. An image is worth 1/2 tokens after layer 2: Plug-and-play inference acceleration for large vision-language models. In *European Conference on Computer Vision*, pages 19–35. Springer, 2024. 7
- [10] Liang Chen, Haozhe Zhao, Tianyu Liu, Shuai Bai, Junyang Lin, Chang Zhou, and Baobao Chang. An image is worth 1/2 tokens after layer 2: Plug-and-play inference acceleration for large vision-language models. In *European Conference on Computer Vision*, pages 19–35. Springer, 2024. 2, 3, 6, 7
- [11] Zesen Cheng, Sicong Leng, Hang Zhang, Yifei Xin, Xin Li, Guanzheng Chen, Yongxin Zhu, Wenqi Zhang, Ziyang Luo, Deli Zhao, et al. Videollama 2: Advancing spatial-temporal modeling and audio understanding in video-llms. *arXiv preprint arXiv:2406.07476*, 2024. 1, 2
- [12] Alexey Dosovitskiy, Lucas Beyer, Alexander Kolesnikov, Dirk Weissenborn, Xiaohua Zhai, Thomas Unterthiner, Mostafa Dehghani, Matthias Minderer, Georg Heigold, Sylvain Gelly, Jakob Uszkoreit, and Neil Houlsby. An image is worth 16x16 words: Transformers for image recognition at scale. In *International Conference on Learning Representations (ICLR)*, 2021. 1
- [13] Jinlan Fu, See-Kiong Ng, Zhengbao Jiang, and Pengfei Liu. Gptscore: Evaluate as you desire. *arXiv preprint arXiv:2302.04166*, 2023. 6
- [14] Mukul Gagrani, Raghav Goel, Wonseok Jeon, Junyoung Park, Mingu Lee, and Christopher Lott. On speculative decoding for multimodal large language models. *arXiv preprint arXiv:2404.08856*, 2024. 2
- [15] Gemini Team, Petko Georgiev, Ving Ian Lei, Ryan Burnell, Libin Bai, Anmol Gulati, Garrett Tanzer, Damien Vincent, Zhufeng Pan, Shibo Wang, et al. Gemini 1.5: Unlocking multimodal understanding across millions of tokens of context. *arXiv preprint arXiv:2403.05530*, 2024. 1, 2
- [16] Albert Gu and Tri Dao. Mamba: Linear-time sequence modeling with selective state spaces. *arXiv preprint arXiv:2312.00752*, 2023. 2
- [17] Zhiyu Guo, Hidetaka Kamigaito, and Taro Watanabe. Attention score is not all you need for token importance indicator in kv cache reduction: Value also matters. *arXiv preprint arXiv:2406.12335*, 2024. 2, 3
- [18] Drew A Hudson and Christopher D Manning. Gqa: A new dataset for real-world visual reasoning and compositional question answering. In *Proceedings of the IEEE/CVF conference on computer vision and pattern recognition*, pages 6700–6709, 2019. 6
- [19] Andreas Krause and Carlos Guestrin. Near-optimal observation selection using submodular functions. In *AAAI*, pages 1650–1654, 2007. 5, 11
- [20] Alex Kulesza, Ben Taskar, et al. Determinantal point processes for machine learning. *Foundations and Trends® in Machine Learning*, 5(2-3):123–286, 2012. 7, 8, 11
- [21] Woojin Kwon, Young Jin Kim, Jiayi Zhang, Shiyang Li, Guanhua Zheng, Ying Sheng Lin, Ion Stoica, Matei Zaharia, and Song Han. Efficient memory management for large language model serving with pagedattention. In *Proceedings of Machine Learning and Systems (MLSys)*, 2023. 2
- [22] Bohao Li, Rui Wang, Guangzhi Wang, Yuying Ge, Yixiao Ge, and Ying Shan. Seed-bench: Benchmarking multimodal llms with generative comprehension. *arXiv preprint arXiv:2307.16125*, 2023. 6
- [23] Wentong Li, Yuqian Yuan, Jian Liu, Dongqi Tang, Song Wang, Jie Qin, Jianke Zhu, and Lei Zhang. Tokenpacker: Efficient visual projector for multimodal llm. *International Journal of Computer Vision*, pages 1–19, 2025. 2, 3
- [24] Yifan Li, Yifan Du, Kun Zhou, Jinpeng Wang, Wayne Xin Zhao, and Ji-Rong Wen. Evaluating object hallucination in large vision-language models. *arXiv preprint arXiv:2305.10355*, 2023. 6
- [25] Bin Lin, Yang Ye, Bin Zhu, Jiayi Cui, Munan Ning, Peng Jin, and Li Yuan. Video-llava: Learning united visual representation by alignment before projection. *arXiv preprint arXiv:2311.10122*, 2023. 1, 2
- [26] Tsung-Yi Lin, Michael Maire, Serge Belongie, James Hays, Pietro Perona, Deva Ramanan, Piotr Dollár, and C Lawrence Zitnick. Microsoft coco: Common objects in context. In *European conference on computer vision*, pages 740–755. Springer, 2014. 6

- [27] Zhihang Lin, Mingbao Lin, Luxi Lin, and Rongrong Ji. Boosting multimodal large language models with visual tokens withdrawal for rapid inference. In *Proceedings of the AAAI Conference on Artificial Intelligence*, pages 5334–5342, 2025. 2, 3, 7
- [28] Zhihang Lin, Mingbao Lin, Luxi Lin, and Rongrong Ji. Boosting multimodal large language models with visual tokens withdrawal for rapid inference. In *Proceedings of the AAAI Conference on Artificial Intelligence*, pages 5334–5342, 2025. 2, 3, 6, 7
- [29] Haotian Liu, Chunyuan Li, Yuheng Li, Bo Li, Yuanhan Zhang, Sheng Shen, and Yong Jae Lee. Llava-next: Improved reasoning, ocr, and world knowledge, 2024. 1, 2, 7
- [30] Haotian Liu, Chunyuan Li, Qingyang Wu, and Yong Jae Lee. Visual instruction tuning. *Advances in neural information processing systems*, 36, 2024. 1, 2, 7
- [31] Yuan Liu, Haodong Duan, Yuanhan Zhang, Bo Li, Songyang Zhang, Wangbo Zhao, Yike Yuan, Jiaqi Wang, Conghui He, Ziwei Liu, et al. Mmbench: Is your multi-modal model an all-around player? In *European conference on computer vision*, pages 216–233. Springer, 2024. 6
- [32] Pan Lu, Swaroop Mishra, Tanglin Xia, Liang Qiu, Kai-Wei Chang, Song-Chun Zhu, Oyvind Tafjord, Peter Clark, and Ashwin Kalyan. Learn to explain: Multimodal reasoning via thought chains for science question answering. *Advances in Neural Information Processing Systems*, 35:2507–2521, 2022. 6
- [33] Kenneth Marino, Mohammad Rastegari, Ali Farhadi, and Roozbeh Mottaghi. Ok-vqa: A visual question answering benchmark requiring external knowledge. In *Proceedings of the IEEE/cvf conference on computer vision and pattern recognition*, pages 3195–3204, 2019. 6
- [34] OpenAI. Gpt-4 technical report. *arXiv preprint arXiv:2303.08774*, 2023. 1
- [35] OpenAI. Hello gpt-4o. <https://openai.com/index/hello-gpt-4o/>, 2024. [Accessed: Nov 2024]. 2
- [36] Kaare Brandt Petersen, Michael Syskind Pedersen, et al. The matrix cookbook. *Technical University of Denmark*, 7(15): 510, 2008. 4
- [37] Bryan A Plummer, Liwei Wang, Chris M Cervantes, Juan C Caicedo, Julia Hockenmaier, and Svetlana Lazebnik. Flickr30k entities: Collecting region-to-phrase correspondences for richer image-to-sentence models. In *Proceedings of the IEEE international conference on computer vision*, pages 2641–2649, 2015. 6
- [38] Yanyuan Qiao, Zheng Yu, Longteng Guo, Sihan Chen, Zijia Zhao, Mingzhen Sun, Qi Wu, and Jing Liu. Vl-mamba: Exploring state space models for multimodal learning. *arXiv preprint arXiv:2403.13600*, 2024. 2
- [39] Alec Radford, Jong Wook Kim, Chris Hallacy, Aditya Ramesh, Gabriel Goh, Sandhini Agarwal, Girish Sastry, Amanda Askell, Pamela Mishkin, Jack Clark, et al. Learning transferable visual models from natural language supervision. In *International conference on machine learning*, pages 8748–8763. PMLR, 2021. 1, 7
- [40] Yuzhang Shang, Mu Cai, Bingxin Xu, Yong Jae Lee, and Yan Yan. Llava-prumerge: Adaptive token reduction for efficient large multimodal models. *ICCV*, 2025. 2, 3, 6, 7
- [41] Mustafa Shukor and Matthieu Cord. Skipping computations in multimodal llms. *arXiv preprint arXiv:2410.09454*, 2024. 2
- [42] Ashish Vaswani, Noam Shazeer, Niki Parmar, Jakob Uszkoreit, Llion Jones, Aidan N Gomez, Lukasz Kaiser, and Illia Polosukhin. Attention is all you need. In *Advances in Neural Information Processing Systems (NeurIPS)*, 2017. 1
- [43] Ramakrishna Vedantam, C Lawrence Zitnick, and Devi Parikh. Cider: Consensus-based image description evaluation. In *Proceedings of the IEEE conference on computer vision and pattern recognition*, pages 4566–4575, 2015. 6
- [44] Jiayi Wang, Zhenyu Zhao, Wei Li, Shuai Han, Chenguang Zhang, and Xing Xie. Soma: Efficient multi-turn llm serving without repeating conversation history. *arXiv preprint arXiv:2501.01234*, 2025. 2
- [45] Yuxin Wang, Shujian Li, Rui Zhao, Xiaoyang Zhou, Tianyu Liu, Min Zhang, and Sujian Li. Cost-efficient large language model serving for multi-turn dialogues with cached attention. *arXiv preprint arXiv:2402.14255*, 2024. 2
- [46] Cong Wei, Yujie Zhong, Haoxian Tan, Yong Liu, Jiawei Hu, Dong Li, and Yujiu Yang. Hyperseg: Hybrid segmentation assistant with fine-grained visual perceiver. In *Proceedings of the IEEE/CVF Conference on Computer Vision and Pattern Recognition (CVPR)*, pages 8931–8941, 2025. 2
- [47] Cong Wei, Yujie Zhong, Haoxian Tan, Yingsen Zeng, Yong Liu, Zheng Zhao, and Yujiu Yang. Instructseg: Unifying instructed visual segmentation with multimodal large language models. In *Proceedings of the IEEE/CVF International Conference on Computer Vision (ICCV)*, pages 1–12, 2025. 2
- [48] Zhibiao Wu and Martha Palmer. Verb semantics and lexical selection. *arXiv preprint cmp-lg/9406033*, 1994. 6
- [49] Shilin Xu, Xiangtai Li, Haobo Yuan, Lu Qi, Yunhai Tong, and Ming-Hsuan Yang. Llava-di: What matters for multimodal large language models distillation. *arXiv preprint arXiv:2407.19409*, 2024. 2
- [50] Weihao Ye, Qiong Wu, Wenhao Lin, and Yiyi Zhou. Fit and prune: Fast and training-free visual token pruning for multimodal large language models. In *Proceedings of the AAAI Conference on Artificial Intelligence*, pages 22128–22136, 2025. 2, 3, 6, 7
- [51] Yaodong Yu, Kwan Ho Ryan Chan, Chong You, Chaobing Song, and Yi Ma. Learning diverse and discriminative representations via the principle of maximal coding rate reduction. *Advances in Neural Information Processing Systems*, 33:9422–9434, 2020. 4
- [52] Zhengqing Yuan, Zhaoxu Li, Weiran Huang, Yanfang Ye, and Lichao Sun. Tinygpt-v: Efficient multimodal large language model via small backbones. *arXiv preprint arXiv:2312.16862*, 2023. 2
- [53] Xiang Yue, Yuansheng Ni, Kai Zhang, Tianyu Zheng, Ruoqi Liu, Ge Zhang, Samuel Stevens, Dongfu Jiang, Weiming Ren, Yuxuan Sun, et al. Mmmu: A massive multi-discipline multimodal understanding and reasoning benchmark for expert agi. In *Proceedings of the IEEE/CVF Conference*

on *Computer Vision and Pattern Recognition*, pages 9556–9567, 2024. 6

- [54] Chi Zhang, Chengjian Feng, Feng Yan, Qiming Zhang, Mingjin Zhang, Yujie Zhong, Jing Zhang, and Lin Ma. Instructvidit: A holistic approach for instructional video editing. *arXiv preprint arXiv:2503.17641*, 2025. 2
- [55] Kaichen Zhang, Bo Li, Peiyuan Zhang, Fanyi Pu, Joshua Adrian Cahyono, Kairui Hu, Shuai Liu, Yuanhan Zhang, Jingkang Yang, Chunyuan Li, et al. Lmms-eval: Reality check on the evaluation of large multimodal models. *arXiv preprint arXiv:2407.12772*, 2024. 7
- [56] Yuanhan Zhang, Bo Li, Haotian Liu, Yong Jae Lee, Liangke Gui, Di Fu, Jiashi Feng, Ziwei Liu, and Chunyuan Li. Llava-next: A strong zero-shot video understanding model. *arXiv preprint arXiv:2405.12107*, 2024. 1, 2
- [57] Yunhang Shen Yulei Qin Mengdan Zhang, Xu Lin Jinrui Yang Xiawu Zheng, Ke Li Xing Sun Yunsheng Wu, Ronrong Ji Chaoyou Fu, and Peixian Chen. Mme: A comprehensive evaluation benchmark for multimodal large language models. *arXiv preprint arXiv:2306.13394*, 18, 2021. 6
- [58] Baichuan Zhou, Ying Hu, Xi Weng, Junlong Jia, Jie Luo, Xien Liu, Ji Wu, and Lei Huang. Tinyllava: A framework of small-scale large multimodal models. *arXiv preprint arXiv:2402.14289*, 2024. 2
- [59] Wenhui Zhu, Xiwen Chen, Zhipeng Wang, Shao Tang, Sayan Ghosh, Xuanzhao Dong, Rajat Koner, and Yalin Wang. Evtptivs: Effective visual token pruning for unifying instruction visual segmentation in multi-modal large language models. *arXiv preprint arXiv:2508.11886*, 2025. 2

A. Proofs

A.1. Proof of Inequality

Recap, for a positive semidefinite square matrix \mathbf{X} , the operator $\Psi(\cdot)$ is presented as:

$$\Psi(\mathbf{X}) = \log \det(\mathbf{I} + \gamma \mathbf{X}) = \sum_{i=1}^d \log(1 + \gamma \lambda_i), \quad (10)$$

where $\{\lambda_i\}$ are the eigenvalues of \mathbf{X} and $\gamma > 0$ is a fixed scaling parameter. Since \mathbf{X} is positive semidefinite (so $\lambda_i \geq 0$), we have the following inequalities,

$$\Psi(\mathbf{X}) \leq \gamma \operatorname{tr}(\mathbf{X}) \leq \gamma (\operatorname{tr}(\mathbf{X}^{1/2}))^2. \quad (11)$$

Now, we will show its proof as follows.

Proof. Let $\mathbf{X} \succeq \mathbf{0}$ with non-negative eigenvalues $\{\lambda_i\}$. For the first inequality in (6), use the elementary bound $\log(1 + t) \leq t$ for all $t \geq 0$. Since $\gamma \lambda_i \geq 0$,

$$\log(1 + \gamma \lambda_i) \leq \gamma \lambda_i \quad \Rightarrow \quad \Psi(\mathbf{X}) \leq \gamma \sum_{i=1}^d \lambda_i = \gamma \operatorname{tr}(\mathbf{X}).$$

For the second inequality in (6), note that

$$\begin{aligned} (\operatorname{tr}(\mathbf{X}^{1/2}))^2 &= \left(\sum_{i=1}^d \sqrt{\lambda_i} \right)^2 \\ &= \sum_{i=1}^d \lambda_i + 2 \sum_{1 \leq i < j \leq d} \sqrt{\lambda_i \lambda_j} \\ &\geq \sum_{i=1}^d \lambda_i = \operatorname{tr}(\mathbf{X}), \end{aligned}$$

because each term $\sqrt{\lambda_i \lambda_j}$ is nonnegative. Multiplying both sides by $\gamma > 0$ gives

$$\gamma \operatorname{tr}(\mathbf{X}) \leq \gamma (\operatorname{tr}(\mathbf{X}^{1/2}))^2.$$

Combining the two inequalities yields

$$\Psi(\mathbf{X}) \leq \gamma \operatorname{tr}(\mathbf{X}) \leq \gamma (\operatorname{tr}(\mathbf{X}^{1/2}))^2,$$

as claimed. \square

A.2. Proof of Submodularity

Definition 1 (Submodularity). A set function $h : 2^{[m]} \rightarrow \mathbb{R}$ is *submodular* if it satisfies the diminishing-returns property: for any $\mathcal{S} \subseteq \mathcal{T} \subseteq [m]$ and any $i \notin \mathcal{T}$,

$$h(\mathcal{S} \cup \{i\}) - h(\mathcal{S}) \geq h(\mathcal{T} \cup \{i\}) - h(\mathcal{T}).$$

Lemma 1. ([5, 19, 20]) Let $\mathbf{A} \in \mathbb{R}^{m \times m}$ be a positive definite matrix, and for any subset $S \subseteq \{1, \dots, m\}$ let \mathbf{A}_S denote the corresponding principal submatrix. Define the set function

$$h(S) = \log \det(\mathbf{A}_S).$$

Then h is a submodular set function.

Proposition 1. Let $\mathbf{V} \in \mathbb{R}^{m \times d}$ and let $\mathbf{V}_{\mathcal{C}}$ denote the submatrix of \mathbf{V} consisting of rows indexed by $\mathcal{C} \subseteq [m]$. Define

$$\Gamma(\mathcal{C}) = \log \det(\mathbf{I} + \tilde{\gamma} \mathbf{V}_{\mathcal{C}} \mathbf{V}^{\top} \mathbf{V} \mathbf{V}_{\mathcal{C}}^{\top}), \quad \tilde{\gamma} > 0.$$

Then Γ is normalized and submodular.

Proof. To prove this proposition, We need to first prove this: Let $\mathbf{V} \in \mathbb{R}^{m \times d}$ be any matrix and $\mathcal{C} \subseteq [m]$ be an index set. Let $\mathbf{V}_{\mathcal{C}}$ denote the submatrix of \mathbf{V} formed by the rows indexed by \mathcal{C} , and let $\tilde{\gamma} \geq 0$. Then the matrix

$$\mathbf{M} = \mathbf{I}_{|\mathcal{C}|} + \tilde{\gamma} \mathbf{V}_{\mathcal{C}} \mathbf{V}^{\top} \mathbf{V} \mathbf{V}_{\mathcal{C}}^{\top} \in \mathbb{R}^{|\mathcal{C}| \times |\mathcal{C}|}$$

is symmetric positive definite.

Since $\mathbf{V}^\top \mathbf{V} \in \mathbb{R}^{d \times d}$ is symmetric positive semidefinite, define

$$\mathbf{A} = \mathbf{V}_C \mathbf{V}^\top \mathbf{V} \mathbf{V}_C^\top \in \mathbb{R}^{|\mathcal{C}| \times |\mathcal{C}|}.$$

We first show that \mathbf{A} is positive semidefinite. For any $\mathbf{x} \in \mathbb{R}^{|\mathcal{C}|}$,

$$\mathbf{x}^\top \mathbf{A} \mathbf{x} = \mathbf{x}^\top \mathbf{V}_C \mathbf{V}^\top \mathbf{V} \mathbf{V}_C^\top \mathbf{x} = (\mathbf{V}_C^\top \mathbf{x})^\top \mathbf{V}^\top \mathbf{V} (\mathbf{V}_C^\top \mathbf{x}).$$

Let $\mathbf{y} = \mathbf{V}_C^\top \mathbf{x} \in \mathbb{R}^d$. Then

$$\mathbf{x}^\top \mathbf{A} \mathbf{x} = \mathbf{y}^\top \mathbf{V}^\top \mathbf{V} \mathbf{y} = \|\mathbf{V} \mathbf{y}\|_2^2 \geq 0,$$

so \mathbf{A} is positive semidefinite.

Now consider

$$\mathbf{M} = \mathbf{I}_{|\mathcal{C}|} + \tilde{\gamma} \mathbf{A}.$$

The matrix \mathbf{M} is symmetric because both $\mathbf{I}_{|\mathcal{C}|}$ and \mathbf{A} are symmetric. For any nonzero $\mathbf{x} \in \mathbb{R}^{|\mathcal{C}|}$ we have

$$\mathbf{x}^\top \mathbf{M} \mathbf{x} = \mathbf{x}^\top \mathbf{I}_{|\mathcal{C}|} \mathbf{x} + \tilde{\gamma} \mathbf{x}^\top \mathbf{A} \mathbf{x} = \|\mathbf{x}\|_2^2 + \tilde{\gamma} \mathbf{x}^\top \mathbf{A} \mathbf{x}.$$

Since \mathbf{A} is positive semidefinite and $\tilde{\gamma} \geq 0$, we have $\mathbf{x}^\top \mathbf{A} \mathbf{x} \geq 0$, so

$$\mathbf{x}^\top \mathbf{M} \mathbf{x} \geq \|\mathbf{x}\|_2^2 > 0$$

for all $\mathbf{x} \neq \mathbf{0}$. Therefore \mathbf{M} is positive definite.

Then we can apply Lemma 1, and we can conclude Γ is sumdoular. \square

B. Detail of Algorithm

In this appendix we describe how our pruning objective naturally leads to the OTPrune algorithm. The derivation begins directly with the token–token interaction matrix and proceeds to the incremental update rules used in Algorithm 1, without introducing additional notation beyond what is necessary.

Given the vision token matrix $\mathbf{V} \in \mathbb{R}^{m \times d}$, we first construct a token–token interaction matrix

$$\tilde{\mathbf{V}} = \mathbf{V} \mathbf{V}^\top \in \mathbb{R}^{m \times m}.$$

The i -th row of this matrix,

$$\mathbf{w}_i^\top = \tilde{\mathbf{V}}[i, :],$$

captures how token i interacts with all other tokens. For a subset $\mathcal{C} \subseteq [m]$, we use

$$\tilde{\mathbf{V}}_C = \tilde{\mathbf{V}}[\mathcal{C}, :]$$

to denote the corresponding row submatrix.

Our pruning objective is the log-determinant

$$\Gamma(\mathcal{C}) = \log \det(\mathbf{I} + \tilde{\gamma} \tilde{\mathbf{V}}_C \tilde{\mathbf{V}}_C^\top), \quad \tilde{\gamma} > 0.$$

This quantity becomes large when the selected interaction vectors $\{\mathbf{w}_i : i \in \mathcal{C}\}$ span a diverse subspace. It is convenient to define the kernel

$$\mathbf{K} = \mathbf{I} + \tilde{\gamma} \tilde{\mathbf{V}} \tilde{\mathbf{V}}^\top, \quad \text{so that} \quad K_{ij} = \delta_{ij} + \tilde{\gamma} \langle \mathbf{w}_i, \mathbf{w}_j \rangle.$$

Here, the Kronecker delta δ_{ij} equals 1 if $i = j$ and 0 otherwise. Then $\Gamma(\mathcal{C}) = \log \det(K_C)$, where K_C is the principal submatrix indexed by \mathcal{C} .

Greedy marginal gain. When considering a new token $j \notin \mathcal{C}$, the determinant of the enlarged matrix can be written using the classical one-step determinant identity:

$$\det(K_{\mathcal{C} \cup \{j\}}) = \det(K_C) \cdot \left(K_{jj} - K_{Cj}^\top K_C^{-1} K_{Cj} \right).$$

Thus the improvement in the objective is

$$\Gamma(\mathcal{C} \cup \{j\}) - \Gamma(\mathcal{C}) = \log d_j^2, \quad d_j^2 = K_{jj} - K_{Cj}^\top K_C^{-1} K_{Cj}.$$

The greedy algorithm simply selects the token with the largest d_j^2 .

Cholesky representation. Let the Cholesky factor of the current kernel submatrix be

$$K_C = LL^\top.$$

Define the coefficient vector

$$\mathbf{c}_j = L^{-1} K_{Cj}.$$

Because $K_C^{-1} = (L^\top)^{-1} L^{-1}$, the quadratic form simplifies to

$$K_{Cj}^\top K_C^{-1} K_{Cj} = \|\mathbf{c}_j\|_2^2,$$

so the greedy score becomes

$$d_j^2 = K_{jj} - \|\mathbf{c}_j\|_2^2.$$

Thus maintaining the greedy scores reduces to tracking \mathbf{c}_i and d_i^2 for all unselected tokens.

Adding a token. Suppose token j is selected. The Cholesky factor of the enlarged set $\mathcal{C} \cup \{j\}$ takes the form

$$L' = \begin{pmatrix} L & 0 \\ \mathbf{c}_j^\top & d_j \end{pmatrix}.$$

For any remaining token $i \notin \mathcal{C} \cup \{j\}$, let the updated coefficient vector be

$$\mathbf{c}'_i = \begin{bmatrix} \mathbf{c}_i \\ e_i \end{bmatrix}.$$

Plugging this into $L'c'_i = K_{\mathcal{C} \cup \{j\}, i}$ yields

$$e_i = \frac{K_{ji} - \langle c_j, c_i \rangle}{d_j}.$$

Once this new coordinate is known, the updated greedy score becomes

$$d_i^2 = K_{ii} - \|c'_i\|^2 = d_i^2 - e_i^2.$$

In general, the update takes the form

$$e_i = \frac{K_{ji} - \langle c_j, c_i \rangle}{d_j}.$$

For our kernel $K_{ji} = \delta_{ji} + \tilde{\gamma} \langle w_j, w_i \rangle$. Since we only update $i \neq j$ (token j has just been selected), the Kronecker delta term vanishes and we obtain

$$e_i = \frac{\tilde{\gamma} \langle w_j, w_i \rangle - \langle c_j, c_i \rangle}{d_j}.$$

This expression exactly the operations executed in Algorithm 1.

Initialization and complexity. With $\mathcal{C} = \emptyset$, all coefficient vectors are empty and the initial scores reduce to

$$d_i^2 = K_{ii} = 1 + \tilde{\gamma} \|w_i\|^2.$$

At iteration t , each of the $(m - t)$ remaining items requires an $O(t)$ inner product $\langle c_j, c_i \rangle$, so the overall cost of the iteration is

$$O((m - t)t).$$

Summing over $t = 1, \dots, k$ gives

$$\sum_{t=1}^k O((m - t)t) = O(mk^2),$$

which is the total complexity of selecting k tokens.

This completes the derivation of *OTPrune* directly from the log-determinant objective.

C. Discussion on Non-uniform Weighting Strategies

In our current framework, we adopt a *uniform weight assumption* for the source distribution P , where each token $v_i \in \mathbf{V}$ is assigned an equal mass of $1/M$. While this simplification allows for a highly efficient and training-free selection process, it treats all visual regions as equally significant, which may not fully capture the semantic variance inherent in complex images.

Potential for Adaptive Importance. Theoretically, the optimal transport formulation in *OTPrune* can be generalized

to accommodate *non-uniform weights* by assigning an importance score w_i to each token, such that $\sum w_i = 1$. As suggested during the rebuttal, such weights could be derived from internal model signals to better reflect semantic density:

- *Attention-based Priors:* Leveraging the cumulative attention weights from preceding transformer layers to identify patches that the model naturally prioritizes.
- *Task-specific Significance:* Utilizing cross-modal alignment scores to assign higher weights to visual tokens that are most relevant to the input text prompt.

Future Challenges. Transitioning to a non-uniform weighting strategy transforms *OTPrune* into a more complex joint optimization problem involving both subset selection and mass allocation. We consider the exploration of *soft-weighted OTPrune*, where token weights are dynamically adjusted during the pruning process—as a promising direction for further improving performance at extremely low pruning ratios.